

IDENTIFICATION OF A TETHERED SATELLITE USING AN EXTENDED
KALMAN FILTER

Except where reference is made to the work of others, the work described in this thesis is my own or was done in collaboration with my advisory committee. This thesis does not include proprietary or classified information.

Elizabeth Jo Volovecky Hayes

Certificate of Approval:

John E. Cochran, Jr.
Professor
Aerospace Engineering

David A. Cicci, Chair
Professor
Aerospace Engineering

Robert S. Gross
Associate Professor
Aerospace Engineering

Joe F. Pittman
Interim Dean
Graduate School

IDENTIFICATION OF A TETHERED SATELLITE USING AN EXTENDED
KALMAN FILTER

Elizabeth Jo Volovecky Hayes

A Thesis

Submitted to

the Graduate Faculty of

Auburn University

in Partial Fulfillment of the

Requirements for the

Degree of

Master of Science

Auburn, Alabama
December 17, 2007

IDENTIFICATION OF A TETHERED SATELLITE USING AN EXTENDED
KALMAN FILTER

Elizabeth Jo Volovecky Hayes

Permission is granted to Auburn University to make copies of this thesis at its discretion, upon the request of individuals or institutions and at their expense. The author reserves all publication rights.

Signature of Author

Date of Graduation

VITA

Elizabeth Jo Volovecky Hayes was born on August 30, 1980 in Fairhope, AL. Her parents are Joe and Debbie (Probst) Volovecky of Daphne, Alabama. Elizabeth graduated from Daphne High School in May of 1998. She enrolled at Auburn University in the fall of 1998, where she began her aerospace studies. Upon receiving her Bachelor of Aerospace Engineering degree in May of 2002, she began her graduate studies in the Aerospace Engineering Department at Auburn the following fall. She married her high school sweetheart, Andy Hayes, in November 2004 and she currently works as an Intel Analyst for SAIC in Huntsville, Alabama.

THESIS ABSTRACT
IDENTIFICATION OF A TETHERED SATELLITE USING AN EXTENDED
KALMAN FILTER

Elizabeth Jo Volovecky Hayes

Master of Science, December 17, 2007
(B.A.E., Auburn University, 2002)

62 Typed Pages

Directed by David A. Cicci

Recent studies involving a tethered satellite system(s) (TSS) have increased due to the importance of accurately identifying and analyzing the motion of a TSS. If the motion of a tethered satellite is not accurately identified, the satellite could be mistaken as a ballistic threat. Standard orbit determination methods used today are unable to identify a tracked satellite as part of a TSS, due to the non-Keplerian nature of its motion.

Accurate identification of a TSS becomes more complicated with the need to perform this process quickly using a small set of observational data. Once this “quick-look” identification process is performed, it is necessary to calculate the critical orbit determination parameters used for future TSS tracking and prediction.

An extended Kalman filter (EKF) has been developed to perform both the state estimation and quick-look identification processes for a tethered satellite not known

a priori as being part of a TSS. In the application of the EKF to a TSS, both, manual tuning and adaptive tuning methods were used. The adaptive tuning method used is based upon ridge-type filtering techniques involving the computation of a biasing parameter that is used as input into the process noise matrix, which is required in tuning the EKF.

The overall performance of the EKF is presented for varying tether lengths, tether orientation, and observation noise levels. The results obtained from the adaptively-tuned EKF are presented in this thesis and are compared to those obtained from a batch filter and manually-tuned EKF presented in recent studies.

ACKNOWLEDGMENTS

I would like to thank my family and friends for being so patient with me throughout my life, but especially through my college journey. You all mean the world to me. I would not be where I am right now without the guidance from the Aerospace Engineering faculty at Auburn University. They have all made a lasting impression in my life. I especially want to thank Dr. David Cicci for all of his patience and understanding through my graduate studies. He never once turned me away even when I thought I asked a “stupid” question and for that, I am most thankful.

Style manual or journal used: *The Journal of the Astronautical Sciences* _____

Computer software used: FORTRAN PowerStation 4.0, Microsoft Excel,
Microsoft Office Word 2003, and Microsoft Equation 3.0 _____

TABLE OF CONTENTS

LIST OF FIGURES	x
LIST OF TABLES	xi
1. INTRODUCTION	1
2. QUICK-LOOK ORBIT DETERMINATION METHOD DESCRIPTION	7
2.1 Preliminary Orbit Determination Method (POD, 1 st Stage)	7
2.2 Identification Using an Extended Kalman Filter (2 nd Stage)	10
2.3 Adaptive Tuning Method Using a Biasing Parameter	14
3. PROCEDURE DESCRIPTION	17
4. TEST CASES	23
5. RESULTS	25
6. CONCLUSIONS	32
REFERENCES	35
APPENDIX A: TEST CASE DATA	37

LIST OF FIGURES

FIG. 1. Tethered Satellite System (TSS) Model	1
FIG. 2. TSS Model with Force Components and Libration Angle	8
FIG. 3. TSS Center-of-Mass and Tether Length Measurements	9

LIST OF TABLES

TABLE 1. Parameter Variations for Scenarios.....	23
TABLE 2. Baseline Orbit for Data Generation.....	23
TABLE 3. Varying Combinations of the Biasing Function	24
TABLE 4. Comparisons for No Tether cases, $\rho_{cm} = 0$ m.....	27
TABLE 5. Comparisons for 1 km cases, $\rho_{cm} = 909$ m, LOW noise.....	28
TABLE 6. Comparisons for 1 km cases, $\rho_{cm} = 909$ m, MEDIUM noise.....	28
TABLE 7. Comparisons for 1 km cases, $\rho_{cm} = 909$ m, HIGH noise	28
TABLE 8. Comparisons for 10 km cases, $\rho_{cm} = 9091$ m, LOW noise	29
TABLE 9. Comparisons for 10 km cases, $\rho_{cm} = 9091$ m, MEDIUM noise.....	29
TABLE 10. Comparisons for 10 km cases, $\rho_{cm} = 9091$ m, HIGH noise	29
TABLE 11. Comparisons for 50 km cases, $\rho_{cm} = 45455$ m, LOW noise	30
TABLE 12. Comparisons for 50 km cases, $\rho_{cm} = 45455$ m, MEDIUM noise.....	30
TABLE 13. Comparisons for 50 km cases, $\rho_{cm} = 45455$ m, HIGH noise	30
TABLE 14. Comparisons for 1 km UP cases, $\rho_{cm} = -909$ m, LOW noise.....	31
TABLE 15. Comparisons for 1 km UP cases, $\rho_{cm} = -909$ m, MEDIUM noise.....	31
TABLE 16. Comparisons for 1 km UP cases, $\rho_{cm} = -909$ m, HIGH noise	31
TABLE 17. Test Case Data: No Tether ($\rho_{cm} = 0$)	38
TABLE 18. Test Case Data: $\rho = 1$ km ($\rho_{cm} = 909$ m), LOW noise	39

TABLE 19. Test Case Data: $\rho = 1$ km ($\rho_{cm} = 909$ m), MEDIUM noise	40
TABLE 20. Test Case Data: $\rho = 1$ km ($\rho_{cm} = 909$ m), HIGH noise	41
TABLE 21. Test Case Data: $\rho = 10$ km ($\rho_{cm} = 9091$ m), LOW noise.....	42
TABLE 22. Test Case Data: $\rho = 10$ km ($\rho_{cm} = 9091$ m), MEDIUM noise	43
TABLE 23. Test Case Data: $\rho = 10$ km ($\rho_{cm} = 9091$ m), HIGH noise.....	44
TABLE 24. Test Case Data: $\rho = 50$ km ($\rho_{cm} = 45455$ m), LOW noise.....	45
TABLE 25. Test Case Data: $\rho = 50$ km ($\rho_{cm} = 45455$ m), MEDIUM noise	46
TABLE 26. Test Case Data: $\rho = 50$ km ($\rho_{cm} = 45455$ m), HIGH noise.....	47
TABLE 27. Test Case Data: $\rho = 1$ km up ($\rho_{cm} = -909$ m), LOW noise	48
TABLE 28. Test Case Data: $\rho = 1$ km up ($\rho_{cm} = -909$ m), MEDIUM noise ..	49
TABLE 29. Test Case Data: $\rho = 1$ km up ($\rho_{cm} = -909$ m), HIGH noise	50

1. INTRODUCTION

A tethered satellite system (TSS) refers to a system that includes two or more satellites, or space bodies, which are connected by a tether, or cord. One idea behind tethered satellites is to control the motion of one satellite by attaching it to another satellite. In a two-bodied TSS, the primary satellite is generally the larger of the two and is referred to as the ‘parent’ satellite. The second satellite, usually smaller than the parent satellite, is referred to as the ‘daughter’ satellite. Either satellite may be located in a higher or a lower orbit with respect to the system’s center-of-mass or they can be in the same orbit. A two-bodied TSS model is shown in Fig. 1 below.

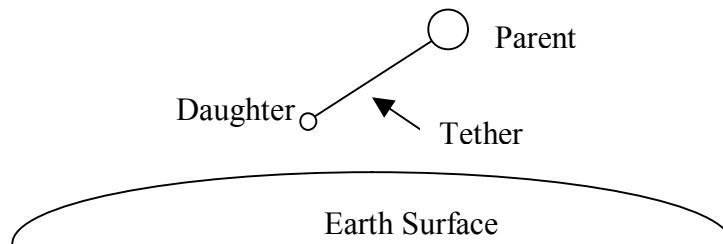


FIG. 1. Tethered Satellite System (TSS) Model

The study of tethered satellites originated in the late 1800’s and has continued on through today with actual ‘in space’ applications. In general, tethered satellites can offer many important uses, such as: providing power between satellites or other space vehicles for transfer of energy or momentum purposes, providing support to astronauts during an

Extra-Vehicular Activity (EVA) maneuver, which connects them to the spacecraft, or providing aid in the control of a space vehicle's motion. It has only been recently that studies have addressed the orbit determination problem of tethered satellites. In one study, a satellite, which was a member of a TSS, was incorrectly identified to be a re-entry object's trajectory [1]. This is due to the tether force perturbing the motion of the tracked satellite and causing it to behave differently than the motion of an untethered satellite [2].

The orbit determination of any space object involves the ability to accurately track, identify, and predict the motion of the object of interest. The need to perform a proper orbit determination analysis of a TSS has increased, since its future use has become important to both the private and public industries. If a TSS is inaccurately analyzed, its motion could result in a tethered satellite being incorrectly identified as a possible threat, resulting in many unnecessary and costly measures being taken to counteract the threat.

It is possible for this type of scenario to occur since tethered satellites behave differently than untethered ones. This is due to the force present in the tether, which acts on all satellites connected to the tether. Each satellite in the TSS is perturbed by the tether force, causing it to vary from the Keplerian-type motion, typically found in untethered satellites [1,2]. When a tethered satellite is stationed in a higher orbit than the center-of-mass of the TSS, its velocity will be larger in magnitude than the results predicted by classical Keplerian motion due to the presence of the tether force. Likewise, if a tethered satellite is in a lower orbit than the center-of-mass of the TSS, its velocity will be smaller than that indicated from classical Keplerian motion due to the tether force.

Classical orbit determination methods are not capable of distinguishing between a tracked tethered satellite and an untethered satellite; therefore the satellite may be incorrectly identified as an untethered one if the classical methods are used. Incorrect identification will also result in an inaccurate prediction of the satellite's future motion.

In order to prevent a TSS from being incorrectly identified, the need to quickly perform the identification process is very important. This process of identification, referred to as "quick-look" identification, is performed by processing measurements of the satellite's motion made from tracking stations. These measurements are acquired by the use of radar, infrared, radio and/or optical techniques and include parameters of the observed satellite, such as: range, range-rate, azimuth, elevation, azimuth-rate and/or elevation-rate. The measurements are then used in the orbit determination process to estimate the satellite's orbit. The first few measurements obtained are used in the preliminary orbit determination (POD) procedure in order to establish a set of initial conditions, which will then be used in the filtering process. In order to more accurately determine the set of initial conditions, a larger set of observational measurements, accumulated from one or more tracking stations, must then be processed.

The need to accurately estimate the state of a tethered satellite, which can include parameters, such as: position, velocity, dynamical constants, etc., involves the differential correction process. Once the POD provides the set of initial conditions, the differential correction process improves the accuracy of the solution acquired by the POD procedure. These improvements are made by processing all of the observational data available in the filtering process. There are several filtering techniques available to use in the differential correction process. The three most commonly used are batch-type filters, Kalman (or

sequential) filters, and extended Kalman (or extended sequential) filters. Batch-type filters process an entire set of observational data at once in order to estimate the state for a specified epoch. Kalman and extended Kalman filters process observations as they are received. A Kalman filter provides the estimate of the satellite's state at each observation time where an extended Kalman filter updates the reference trajectory at each observation to reflect the best estimate of the true trajectory. Each filter has its distinct advantages and disadvantages; however this study will utilize the extended Kalman Filter (EKF) and compare its results to previous studies using batch-type and sequential estimators.

A POD method was recently developed [3,4] for the use of both tethered and untethered satellites. Following this method, several different batch-type filters for the estimation of the state of a tethered satellite were presented and their performances were compared [5]. In this study a two-dimensional dynamical model of a TSS was considered. The model maintained a vertical orientation and as a result did not possess the capabilities to include out-of-plane motion of the system, or any apparent oscillatory motion of the TSS. There have been additional studies where out-of-plane libration of a TSS was modeled, in an enhanced batch filter [6].

The accuracy of quick-look TSS identification was improved by the use of ridge-type estimation methods [7]. Once a satellite is identified as being a tethered satellite, more sophisticated models of a TSS [8-12] can then be used to predict its long-term motion. When long arcs of observational data are available, these enhanced dynamical models and filtering techniques are more useful.

A more recent presentation involved a method that combined all of the desired characteristics needed in both the quick identification and the prediction of long-term

motion of a TSS. The three-stage TSS identification and orbit determination methodology [13] included: a 1st Stage POD procedure, a 2nd Stage ridge-type filter, and a 3rd Stage long-term prediction filter. The performance of this methodology was demonstrated using a series of simulated cases with varying TSS geometry and observation noise levels, as well as on real TSS data obtained from the Tether Physics and Survivability Experiment (TiPS) [14].

An extended Kalman filter (EKF) was recently developed in order to address the TSS identification problem using extended sequential processing of the observational data [15]. The primary emphasis is on the quick-look aspects of tethered satellite identification rather than on the long-term orbit prediction aspects referred to in [13]. The manually-tuned EKF utilizes the POD results from [13] as initial conditions, and short arcs of observations are processed in order to determine the best estimate of the satellite's state. The performance of the EKF is evaluated through the analysis of simulated data using differing tether lengths, tether orientations, observational error levels, and observation arcs.

An adaptive or automated tuning methodology, used in angles-only tracking and intercept problems [16], was applied to the EKF to improve overall filter performance and to make the entire filtering process less tedious. The tuning method involves the use of a biasing parameter that is computed within the EKF. The biasing parameter is an integral part of ridge-type estimation techniques, which have shown improved accuracy in batch and sequential solutions of ill-conditioned orbit determination problems. The biasing parameter provides a measure of the overall solution error and is input into the process noise matrix for tuning the EKF. The performance of the filter depends on

correct propagation of the covariance matrix added with the *a priori* covariance, the observational covariance, and the process noise [16]. A “tuned” extended Kalman filter means that the best possible filter performance is achieved.

The elements of the process noise covariance and measurement noise covariance matrices need to be properly determined through the tuning process in order to improve the filter’s ability to provide accurate state estimates. The results from the adaptively-tuned EKF are presented in this study and are compared to the results obtained using the batch filter from the 2nd Stage of the TSS methodology presented in [13] along with those results from the manually-tuned EKF presented in [15]. Conclusions for their use are also provided.

2. QUICK-LOOK ORBIT DETERMINATION METHOD DESCRIPTION

The suggested orbit determination method for TSS involves two different dynamic models. The first stage of the methodology is a POD strategy that uses a simple dynamic model, while an enhanced dynamic model is used in the EKF of the second stage quick-look identification process. The related TSS models are specifically designed for those stages in order to yield the most accurate results for a given span of observations. The 1st Stage uses only a few observations in its process where the results are used as input into the 2nd Stage. The 2nd Stage performs an adaptive, sequential analysis using up to 15 minutes of the observational data. Each stage, along with their models, is described in more detail in the following paragraphs.

2.1 Preliminary Orbit Determination (POD, 1st Stage)

The TSS model used in the POD stage consists of a ‘daughter’ satellite, m , and a ‘parent’ satellite, m_p , where both are considered to be point masses. These satellites are connected by a massless tether, as illustrated in Fig. 2. Also shown in Fig. 2, is the effective tether force that acts upon the daughter satellite. The radial and tangential force components, F_r and F_t , respectively, which make up the tether force, are shown acting on the daughter satellite, since its motion is the one being observed. Depending on where the satellites are located in their orbit and in relation to each other, their velocities will be affected due to the change in acceleration imposed by the force components. For

example, the radial force component will create a radial acceleration, a_r , which acts on the daughter satellite, and will cause its velocity to decrease if it lies in a lower orbit than the parent satellite, and will cause its velocity to increase if it lies in a higher orbit than the parent satellite, but will cause its velocity to increase if it lies in a higher orbit than the parent satellite. Likewise, the tangential force component will create a tangential acceleration, a_t , on the daughter, causing its velocity to decrease if it precedes the parent, but causing its velocity to increase if it trails the parent. In the case where the parent satellite is being observed, the opposite of these dynamical characteristics will be true.

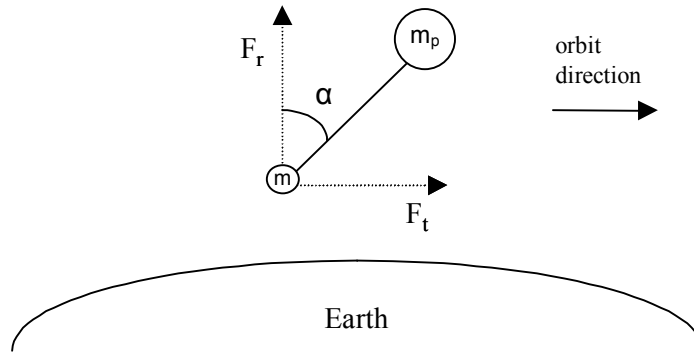


FIG. 2. TSS Model with Force Components and Libration Angle

One satellite preceding or ‘leading’ another satellite depends on the in-plane libration angle, α , as shown in Fig. 2. The value of α will also determine the directions of the tether force components, where the positive radial direction is defined from the center of Earth toward the daughter satellite and the positive tangential direction is that of the direction of orbital motion.

The radial acceleration of a satellite’s motion can be obtained using a POD method along with other information, including the gravitational parameter, μ .

Specifically, a modified gravitational parameter, μ^* , can be calculated during the POD process by a relationship between the parameters μ and a_r , which is presented in [3,4] as:

$$\mu^* = \mu - a_r r^2 \quad (2.1)$$

Where, r , is the distance from the center of the Earth to the daughter satellite. Upon obtaining μ^* , it can be used to find an approximate value of the distance from the daughter satellite to the center-of-mass of the TSS, which is designated by, ρ_{cm} , and illustrated in Fig. 3..

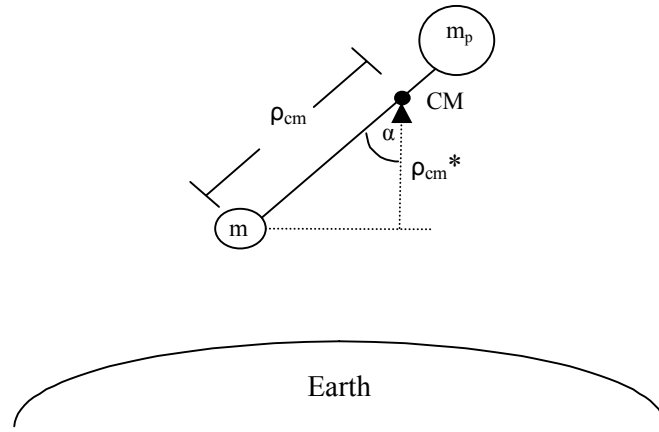


FIG. 3. TSS Center-of-Mass and Tether Length Measurements

This distance is measured along the tether length and can illustrate whether the daughter satellite is above or below the parent satellite. When libration is present in the TSS, ρ_{cm} will represent the projection of the tether length (to the center-of-mass) in the radial direction and will be denoted by the parameter, ρ_{cm}^* , and is presented in [3,4] as:

$$\rho_{cm}^* = \left[\frac{(\mu - \mu^*)}{2\mu + \mu^*} \right] r \quad (2.2)$$

If ρ_{cm}^* is positive, then the daughter satellite is below the parent and $\mu^* < \mu$. If it is negative, then the daughter is above the parent satellite where $\mu^* > \mu$, which indicates that the satellite being observed is above the parent satellite. In addition, the value of ρ_{cm} will approach the actual tether length as the ratio of the point masses, m/m_p , approaches zero.

Several classical POD methods were modified to include the capabilities to determine μ^* for a TSS and were presented in [3,4]. Due to superior convergence characteristics, the 9th order f and g series method proved to perform best and those results were used in this study. The calculated value of μ^* can be used quickly to determine whether the observed satellite is part of a TSS due to the few observations that are used in the POD process. The output from the 1st Stage POD method, in the form of position, velocity, and a_r , is used as input into the 2nd Stage Extended Kalman Filter. The POD results provide no information regarding a_t , therefore a_t is initially assumed to be zero.

2.2 Identification Using an Extended Kalman Filter (2nd Stage)

The enhanced dynamical TSS model used in the “quick-look” identification process, presented in [6], is similar to the model presented in the 1st Stage, but includes additional dynamical effects. The model for the 2nd Stage considers the tether to be inextensible and allows for oblate Earth effects, as well as, in-plane libration in the TSS dynamics.

To determine the dynamical TSS characteristics, including: acceleration components, libration angle, etc., a batch-type filter has been used [5] to generate an

estimation of the daughter satellite's state vector. This state vector includes the satellite's position and velocity components and the acceleration components due to the tether force. The acceleration components, a_r and a_t , are both assumed to be constant over short observation arcs. This implies that the libration angle will remain constant through the observation arc as well. Since these parameters are tether-specific, including them in the filter allows for the satellite to be identified as tethered or untethered. A satellite is found to be untethered when its acceleration components are determined to be zero. This means that there is no tether force perturbing the acceleration components. Likewise, nonzero acceleration terms indicate that the satellite being observed is tethered. No other forces, such as: thrust, drag, which creates orbit decay, etc. are considered in this study. Once the acceleration terms are obtained, they can be used to calculate the libration angle of the TSS.

In order to perform the 2nd Stage process in a sequential manner, an extended Kalman filter (EKF) is used to quickly identify the observed satellite with a short arc of observational data. Classic EKF equations are used in this study and are explained in more detail below. To better describe the EKF, it is appropriate to summarize the process of the Kalman (or sequential) filter first and then provide a comparison. Swerling originally developed the sequential algorithm in 1958 [17], yet Kalman and Bucy have been recognized more for their work with the algorithm since 1961 [18]. The most important difference between the two filters is that the sequential algorithm processes observational data as it is received, while the EKF does the same and in addition, updates the reference trajectory after each observation is processed. The disadvantage of the sequential algorithm is the significant amount of errors due to neglecting higher order

terms in the linearization procedure. The EKF is used to decrease the effects of those errors, which allows for more rapid convergence. When using the sequential algorithm, if the true trajectory and the reference trajectory are too far apart, which is often the case at the beginning of a simulation, the estimation process may diverge due to the errors from the linearization process, previously described. The benefit in using the EKF is that the best estimate of the state will be reached more quickly. Below is a description of the EKF algorithm:

1. Given the following:

- \hat{X}_{k-1} , the estimate of the state vector at t_{k-1} , ($n \times 1$);
- P_{k-1} , covariance matrix at time t_{k-1} , ($n \times n$);
- Y_k , p -vector of observations taken at time t_k , ($p \times 1$);
- R_k , observation covariance at time t_k , ($p \times p$);

2. Integrate from t_{k-1} to t_k ,

$$\dot{\bar{X}} = F(\bar{X}(t), t), \quad \bar{X}(t_{k-1}) = \hat{X}_{k-1} \quad (2.3)$$

$$A(t) = \frac{\partial F(\bar{X}(t), t)}{\partial X(t)} \quad (2.4)$$

$$\dot{\bar{P}}_k = A(t)P_{k-1} + P_{k-1}A^T(t) + Q(t) \quad (2.5)$$

where $\bar{X}(t)$ is the updated state vector ($n \times 1$), $F(\bar{X}(t), t)$ is the system dynamics function ($n \times 1$), $A(t)$ is the state sensitivity matrix ($n \times n$), and where $Q(t)$ is the process noise matrix ($n \times n$).

3. Compute,

$$H_k = \frac{\partial G(\bar{X}(t_k), t_k)}{\partial \bar{X}(t_k)} \quad (2.6)$$

$$K_k = \bar{P}_k H_k^T (H_k \bar{P}_k H_k^T + R_k)^{-1} \quad (2.7)$$

$$P_k = (I - K_k H_k) \bar{P}_k \quad (2.8)$$

$$y_k = Y_k - G(\bar{X}(t_k), t_k) \quad (2.9)$$

$$\hat{x}_k = K_k y_k \quad (2.10)$$

$$\hat{X}_k = \bar{X}_k + \hat{x}_k \quad (2.11)$$

where H_k is the measurement sensitivity matrix ($p \times n$), $G(\bar{X}(t_k), t_k)$ is the observation-state relationship vector ($p \times 1$), K_k is the Kalman gain ($n \times p$), P_k is the covariance matrix ($n \times n$) associated with the best estimate of the ($n \times 1$) state vector \hat{X}_k , y_k is the observation residual vector ($p \times 1$), Y_k is the current observation, and \hat{x}_k is the state correction vector ($n \times 1$). All variables are computed at time t_k .

4. Replace k with $k-1$, return to step 2 and substitute. Repeat until all observations have been read.

The algorithm above assumes that the process noise matrix, $Q(t)$, is known. This will be discussed in more detail in the following section.

The state vector, \hat{X}_k , used in the 2nd Stage process will include the observed satellite's position, velocity, and tether acceleration components. Upon obtaining the initial estimate of the state vector at each observation time, several determinations can be made relative to the tether acceleration components [13], such as:

1. If the values of a_r and a_t are found to be zero, it can be assumed that the observed satellite is an untethered one and standard techniques can be used to analyze its motion.
2. If the values of a_r and a_t are nonzero, then the following applies:
 - a. The libration angle, α , can be calculated from,

$$\alpha = \tan^{-1} \left(\frac{a_t}{a_r} \right) \quad (2.12)$$

where the signs of a_r and a_t will determine the appropriate quadrant for α .

- b. The magnitude of the acceleration due to the tether force can be calculated from,

$$\frac{F_T}{m} = \sqrt{(a_r^2 + a_t^2)} \quad (2.13)$$

- c. The value of ρ_{cm}^* , the radial projection of the tether length to the center-of-mass of the TSS, can be approximated through the use of a_r and Equations 2.1 and 2.2.
3. In the case where one of the acceleration components is equal to zero and the other is not, then the following applies:
- a. For $a_t = 0$ and $a_r \neq 0$, the satellite will be tethered and the system's orientation will be vertical. This will be the case when $\alpha = 0^\circ$ and $a_r > 0$ or when $\alpha = 180^\circ$ and $a_r < 0$.
- b. For $a_r = 0$ and $a_t \neq 0$, the satellite will be tethered and the system's orientation will be horizontal. This will be the case when $\alpha = 90^\circ$ and $a_t > 0$ or when $\alpha = 270^\circ$ and $a_t < 0$.

The methodology from the 2nd Stage process combined with the implementation of the tuning method described in the following section will complete the quick look identification method.

2.3 Adaptive Tuning Method using a Biasing Parameter

Before describing the adaptive tuning algorithm it is appropriate to stress the importance of “tuning” an EKF in general. An EKF must be properly tuned in order to prevent filter divergence. This is achieved by adding adequate values of the *a priori* covariance and the observational covariance, if known, to the propagation of the covariance to properly generate the filter's performance envelope; any “process noise” is also added. A major disadvantage to tuning an EKF is that the results are usually

achieved manually, which is very tedious and allows for significant error. These problems present the need for an aid which “automatically” tunes an EKF. In this presentation, an adaptive tuning method presented by Cicci [16], typically used in angles-only tracking and intercept problems, was applied to the EKF described in the previous section; yielding an adaptively-tuned EKF.

The adaptive tuning method used in this study is based upon ridge-type estimation methods and requires the calculation of a biasing parameter, which represents the overall error in the solution and is used as input into the process noise matrix. The process noise matrix, $Q(t)$, defined above in the 2nd Stage description, is necessary to successfully tune the EKF and can be expressed as a function of the biasing parameter and written as $Q(k)$, as described by Cicci [16]. The biasing parameter provides the following advantages to the EKF:

1. The diagonal terms of the process noise matrix are updated after each observation time as opposed to remaining constant for all of the observations.
2. Adaptive tuning allows the user to define how the biasing parameter is implemented at the beginning of the simulation, eliminating manual changes to the process noise.

The form of the biasing parameter, k , is determined through converting the batch solution into a sequential solution, described in [16]. The sequential form of the biasing parameter, k , is presented below:

$$k = \frac{\text{tr}(D_m R D_m)^2 + \hat{x}^T H^T D_m^{-2} (D_m R D_m)^2 [2(D_m R D_m) + I_m] H \hat{x}}{\hat{x}^T H^T D_m^{-2} (D_m R D_m)^2 [D_m R D_m + I_m] H \hat{x}} \quad (2.14)$$

where D_m is a normalizing diagonal matrix ($p \times p$) and its i th diagonal term is defined as:

$$D_m = \frac{1}{\sqrt{HPH^T}} \quad (2.15)$$

As stated in [16], the inspection of equation 2.14 above shows that k will always be greater than one. As the covariance matrix, \bar{P} , decreases with each processed observation, the biasing parameter, k , also decreases in value and approaches one. As described before, k represents the overall error in the solution and $Q(t)$ represents the process noise, therefore k is used to compute the $Q(k)$ matrix, which includes the effects of k -biasing. With each observation k is computed and then used to update the appropriate $Q(k)$ terms. Only those $Q(k)$ terms that will effect the acceleration terms of the propagated covariance matrix [16] will be updated with the biasing parameter, since that is where most of the error exists.

In summary, the description of the biasing parameter and its use within the EKF concludes the quick-look orbit determination process. Implementation of the process, test cases and results are described in the following sections.

3. PROCEDURE DESCRIPTION

At this point it is necessary to expand on the methods previously explained by summarizing the overall procedure that was implemented in this thesis study. Beginning with the POD (1st Stage) process, only the output data obtained from the POD presentations referenced in [3,4] was used as input into the adaptive EKF (2nd Stage); no additional POD processes were considered. The output data from the POD process provides a reference trajectory for the tracked satellite with results in the form of the position vector, \bar{R} , velocity vector, \bar{V} , and μ^* , which includes the standard gravitational parameter, μ , and the radial acceleration tether force component acting on the satellite. Using equation 2.1, this radial acceleration component, a_r , can be calculated since the remaining variables are known. With the zero tangential acceleration component, a_t , these parameters form the starting state vector for the daughter satellite which is used as input into the EKF (2nd Stage).

To implement the adaptive EKF in this study, the FORTRAN program developed for [15] was modified to include the adaptive parameters. The entire estimation process used in this study will be described in the paragraphs below, however the form that the state vector assumes for this study, must be explained first. The state vector includes the parameters from the POD process, satellite position, velocity, and acting tether

acceleration force. The state variables related to the dynamics of the satellite's motion are defined in equation 2.16, below:

$$\bar{X} = \bar{X}(t) = \begin{bmatrix} x \\ y \\ z \\ \dot{x} \\ \dot{y} \\ \dot{z} \\ a_t \\ a_r \end{bmatrix} = \begin{bmatrix} X_1 \\ X_2 \\ X_3 \\ X_4 \\ X_5 \\ X_6 \\ X_7 \\ X_8 \end{bmatrix} \quad (2.16)$$

The equation of motion, including perturbation effects acting on the satellite, used in this study and those being compared to this study, is provided in equation 2.17. Definitions of the perturbation forces, \bar{p} , which represents the effects of oblateness, and, \bar{F}_t , which represents the tether acceleration effects on the satellite, are provided in equations 2.18 and 2.19, respectively.

$$\ddot{\bar{R}} = \frac{-\mu\bar{R}}{R^3} + \bar{p} + \bar{F}_t \quad (2.17)$$

$$\bar{p} = \frac{\mu J_2 R_e^2}{2R^3} \left(1 - \frac{3z^2}{R^2} \right) \quad (2.18)$$

$$\bar{F}_t = \frac{a_r \bar{R}}{R} + \frac{a_t \bar{V}}{V} \quad (2.19)$$

In equation 2.18, J_2 is the oblateness constant coefficient, R_e is the radius of the earth, and z is the z -component of the satellite's position. In equation 2.19, a_r and a_t represents the satellite's radial and tangential tether force acceleration terms, respectively. R and V are the magnitudes of the satellite's position and velocity, respectively.

Take the time derivative of the state vector dynamics to find $\dot{\bar{X}}$ and substitute equations 2.17-2.19; yielding equation 2.20, where \bar{X} is a function of the state variables.

$$\dot{\bar{X}} = F(\bar{X}(t), t) = \begin{bmatrix} \dot{X}_1 \\ \dot{X}_2 \\ \dot{X}_3 \\ \dot{X}_4 \\ \dot{X}_5 \\ \dot{X}_6 \\ \dot{X}_7 \\ \dot{X}_8 \end{bmatrix} = \begin{bmatrix} X_4 \\ X_5 \\ X_6 \\ \left(\frac{X_1 \mu}{R^3} \right) \left(-1 - \frac{3J_2 R_E^2}{2R^2} + \frac{15J_2 R_E^2 X_3^2}{2R^4} \right) + \frac{X_8 X_1}{R} + \frac{X_7 X_4}{V} \\ \left(\frac{X_2 \mu}{R^3} \right) \left(-1 - \frac{3J_2 R_E^2}{2R^2} + \frac{15J_2 R_E^2 X_3^2}{2R^4} \right) + \frac{X_8 X_2}{R} + \frac{X_7 X_5}{V} \\ \left(\frac{X_3 \mu}{R^3} \right) \left(-1 - \frac{9J_2 R_E^2}{2R^2} + \frac{15J_2 R_E^2 X_3^2}{2R^4} \right) + \frac{X_8 X_3}{R} + \frac{X_7 X_6}{V} \\ 0 \\ 0 \end{bmatrix} \quad (2.20)$$

The observation vector, y , as defined in equation 2.9 requires the use of an observation-state relationship vector, $G(\bar{X}(t), t)$, defined here in equation 2.21.

$$\begin{aligned} G_1 &= \sqrt{(X_1 \cos \theta + X_2 \sin \theta - X_s)^2 + (-X_1 \sin \theta + X_2 \cos \theta - Y_s)^2 + (X_3 - Z_s)^2} \\ G_2 &= a \tan \left(\frac{(-X_1 \sin \theta + X_2 \cos \theta - Y_s) \cos \lambda - (X_1 \cos \theta + X_2 \sin \theta - X_s) \sin \lambda}{(X_1 \cos \theta + X_2 \sin \theta - X_s) \sin \phi \cos \lambda + (-X_1 \sin \theta + X_2 \cos \theta - Y_s) \sin \phi \sin \lambda - (X_3 - Z_s) \cos \phi} \right) \\ G_3 &= a \sin \left(\frac{(X_1 \cos \theta + X_2 \sin \theta - X_s) \cos \phi \cos \lambda + (X_3 - Z_s) \sin \phi + (-X_1 \sin \theta + X_2 \cos \theta - Y_s) \cos \phi \sin \lambda}{\sqrt{(X_1 \cos \theta + X_2 \sin \theta - X_s)^2 + (-X_1 \sin \theta + X_2 \cos \theta - Y_s)^2 + (X_3 - Z_s)^2}} \right) \end{aligned} \quad (2.21)$$

In equation 2.9, Y , represents the current observation's range, azimuth, and elevation values of the satellite as measured relative to the tracking station. In equation 2.21, θ is equal to the ω_E at the current observation time. X_s , Y_s , and Z_s are the known position parameters (in Earth-Centered Earth Fixed, ECEF) for the tracking station location. The latitude and longitude of the tracking station, also known, are ϕ and λ , respectively. The observation vector equations include the transformations between the tracking station's local coordinate frame and the ECEF coordinate frame.

The equations provided for $\dot{\bar{X}}$ and the observation vector, y , were also used in presentations [3,4,15]. They are used in this study to provide consistency for comparing results from test cases.

After explaining the forms of the state and observation vectors, the simulation description proceeds. Initially, the diagonal values for the *a priori* covariance and process noise matrices are given to begin the quick-look EKF analysis. The values for the *a priori* covariance matrix used in this thesis will be explained in more detail in the Test Cases section.

1. First, the state estimate found from the POD results are read into the program. Processing one observation at a time, in 5 second intervals and up to 15 minutes of data, the range, azimuth, and elevation defining the satellite's location relative to the tracking station is recorded. Also processed is the observation covariance.
2. Compute EKF equations 2.5 through 2.10 and calculate the predicted state vector and covariance matrix (with process noise and the k-biasing function).
3. Update the state estimate and *a priori* covariance matrix.
4. Calculate the Root Mean Square (RMS).
5. Calculate ρ_{cm}^* using equation 2.2.
6. Begin processing the next observation with the updated state estimate and process noise matrix and continue until all observations are processed.

Once the k-biasing parameter is calculated using equation 2.14 it is used in a biasing function to update the appropriate terms of the process noise matrix for use in the next observation. The Root Mean Square (RMS) is also calculated at each observation to measure any process error, which aids in identifying the convergence of the best solution. The projection of the tether length (to the center-of-mass) in the radial direction, ρ_{cm}^* , is

then calculated. The next observation is processed using the updated process noise matrix (with biasing included) and the best estimate of the state vector. This procedure continues until all observations are processed.

In this study, those terms in the process noise matrix that effect the tether acceleration components will be the only terms considered. These terms are functions of the k -biasing parameter used to automatically tune, or adjust, the propagation of the state covariance matrix.

As mentioned before, the process noise matrix, $Q(k)$, is updated with functions of the k -biasing parameter. Only the acceleration terms of the matrix will be updated as shown in the following form.

$$Q(k) = \begin{bmatrix} 0 & 0 & 0 & 0 & 0 & 0 & 0 & 0 \\ 0 & 0 & 0 & 0 & 0 & 0 & 0 & 0 \\ 0 & 0 & 0 & 0 & 0 & 0 & 0 & 0 \\ 0 & 0 & 0 & 0 & 0 & 0 & 0 & 0 \\ 0 & 0 & 0 & 0 & 0 & 0 & 0 & 0 \\ 0 & 0 & 0 & 0 & 0 & 0 & 0 & 0 \\ 0 & 0 & 0 & 0 & 0 & 0 & f_1(k) & 0 \\ 0 & 0 & 0 & 0 & 0 & 0 & 0 & f_2(k) \end{bmatrix} \quad (2.22)$$

The functions used for $f_1(k)$ and $f_2(k)$ are dependent upon the types of scenarios that are being analyzed. There are no limitations to the types of function that can be used, but some effort may need to be put forth at the beginning of the analysis to make sure the appropriate functions are chosen to use. For instance, in angles-only tracking intercept problems, the functions should be chosen so that larger values of the process noise are provided to the components that contain high levels of error [16]. Other cases may not include levels of error that are significantly high; requiring a biasing function to yield smaller values.

Using the biasing function in the process noise matrix, which is updated at each observation, should provide faster tuning results to the EKF. This allows the EKF to perform more powerfully and with high confidence of the best converging solution.

4. TEST CASES

Many different scenarios were considered in this thesis study to illustrate the adaptive EKF's performance when identifying whether the observed satellite is tethered or untethered. In the end, over 2,000 scenarios were generated to test the EKF. This involved scenarios, limited to the data provided from simulated data acquired from a previous study [3], with varying tether lengths, orientations, observation noise levels, and observation arcs; specific values and levels are summarized in Table 1 below.

TABLE 1. Parameter Variations for Scenarios

Tether Lengths (ρ)	0 km, 1 km, 10 km, 50 km, and 1 km UP
Orientation: In-Plane Libration Angle (α)	0°, 5°, 10° (N/A for 0 km cases)
Observation Noise Levels	LOW (5 m/0.002°), MEDIUM (25 m/0.01°), and HIGH (50 m/0.02°)
Observation Arcs	5, 10, and 15 minutes

The simulated data was generated using a baseline circular orbit [3]. The orbital elements for this circular orbit are provided in Table 2 below.

TABLE 2. Baseline Orbit for Data Generation

Orbital Elements	
a	6621 km
e	0.00
i	5.73 deg
Ω	5.73 deg

Each test case scenario used as input the *a priori* covariance matrix found with the best manually-tuned results from the EKF presented in [15]. The idea behind this is to provide commonality among both filters for comparison purposes and to ultimately determine which filter yielded faster and more accurate results.

As mentioned when describing the procedure for implementing all presented methodology in this study, many combinations for the k -biasing function, used in the process noise matrix, $Q(k)$, were also considered. Some of the functions used were taken from [16], in order to provide a common foundation for comparing results to the adaptive EKF. A description of the combinations used in the k -biasing functions is presented in Table 3 below.

TABLE 3. Varying Combinations of the Biasing Function

Functions used for both, $f_1(k)$ & $f_2(k)$	
k and k^2 , from [16]	$\frac{1}{k^n}$, where $n = 1, 2, 3, 4, \dots, 21$
$(k-1)$ and $(k-1)^2$, from [16]	$\frac{1}{(k-1)^n}$, where $n = 1, 2, 3, 4, \dots, 9$
$(k+1)$ and $(k+1)^2$	$\frac{1}{(k+1)^n}$, where $n = 1, 2, 3, 4, \dots, 21$

The results from the two best biasing functions from [16] and two from the remaining combinations from Table 3 are presented for all test case scenarios in Appendix A. The same function is not ideal for all test cases due to observation, process, and user errors. Out of the four cases presented for each test case scenario, the case yielding the best solution represents optimum results found from the adaptive EKF for that test case.

5. RESULTS

From the results presented for each test case in Appendix A, a variety of different combinations of biasing functions were used to acquire the end results for this study. The best solutions from these test cases were taken and compared to the best solutions from the batch filter presented in [13] and the manually-tuned EKF presented in [16]. Tables 4 through 16 organize this information from all three studies so that appropriate conclusions may be drawn.

Overall the adaptive EKF produced the most accurate results within 15 minutes of observed data for all tether lengths and k-biasing functions presented. The tables of data provided observe the adaptive EKF's performance at three different time spans (5, 10, and 15 minutes); this provides the opportunity to monitor whether or not a test case converges sooner than the anticipated 15 minute time span. Where this occurred, which was in very few cases, it was determined that the early convergence was due to the proper selection of the biasing function. Additionally, the rapid divergence that was found in the following time span, for these cases, demonstrated that the best solution had already occurred for the test case.

The adaptive EKF was able to produce the best results for the no tether cases within 10 minutes of data and to match those of the manually-tuned EKF. The cause for

this result illustrates the ability to choose the biasing function to achieve the desired results. In these cases, the process noise matrix values were zero for the manually-tuned EKF, therefore the biasing function used in the adaptive EKF needed to provide small values for the process noise so that the solutions would be similar when compared. This means that the value of k needed to be larger when using a function similar in form to $(k + 1)^{-n}$, where n is larger; the output from this biasing function is driven to the expected limit, or floor, more quickly.

The adaptively-tuned EKF was more sensitive to observation error and libration levels than those results found from the manually-tuned EKF. Results from the adaptive-tuned EKF for test cases with high noise levels performed better than the low and medium noise level cases for some tether lengths. In the cases where low levels of noise were present the results varied depending on the amount of libration present. Higher amounts of libration provided better results (i.e. RMS closest to 1 and ρ_{cm}^* closest to desired value) for these cases.

Results from the adaptively-tuned EKF became more accurate with higher tether lengths, which did not seem to have an affect in either the batch filter or manually-tuned EKF processes. In all three filter cases, there was commonality among the no tether cases diverging as observation noise increased.

The amount of error the input conditions and process noise are expected to contain, aids in selecting the “best” biasing function to use. Varying the k -biasing function provided a unique look into the overall convergence to the best solution for each case. Because many biasing functions were considered for each scenario in this study, selecting the biasing function that provided the best solution to each test case was simple.

As verification that the best solution had been achieved, the very next variation of the biasing function used in the scenario, and any thereafter, provided an immediate and significant divergence. This pattern provided confidence throughout the entire adaptively-tuned EKF analysis that the best solution for each test case had been determined.

The RMS values calculated at each observation and recorded for all three time spans provided good results in most of the cases. Where the RMS values were significantly higher than the ideal value of one, the conclusion is that the adaptively-tuned EKF procedure required more observations, than either the batch or manually-tuned EKF processes needed, to find the best converged solution.

TABLE 4. Comparisons for No Tether cases, $\rho_{cm} = 0$ m

σ	Δt	Batch Filter [13]		Manually-tuned EKF [16]		Adaptively-tuned EKF with k -biasing	
		RMS	$\rho_{cm}^*(m)$	RMS	$\rho_{cm}^*(m)$	RMS	$\rho_{cm}^*(m)$
low	5 min:	1.021	-116	0.243	-2416	0.2431	-2416
	10 min:	1.025	310	0.443	-39	0.4433	-39
	15 min:	1.006	152	0.686	92	0.6862	92
med	5 min:	1.042	4246	0.233	-6559	0.2329	-6559
	10 min:	1.021	624	0.363	320	0.3631	320
	15 min:	1.011	708	0.709	685	0.7086	685
high	5 min:	1.033	4613	0.188	-9622	0.1879	-9622
	10 min:	1.021	1400	0.362	551	0.3622	551
	15 min:	1.009	1493	0.706	1297	0.7059	1297

TABLE 5. Comparisons for 1 km cases, $\rho_{cm} = 909$ m, LOW noise

		Batch Filter [13]		Manually-tuned EKF [16]		Adaptively-tuned EKF with k -biasing	
α	Δt	RMS	ρ_{cm}^* (m)	RMS	ρ_{cm}^* (m)	RMS	ρ_{cm}^* (m)
0°	5 min:	1.022	277	13.211	-233381	16.03	30885
	10 min:	1.022	991	3.218	9275	7.760	30051
	15 min:	1.007	1077	0.570	1227	4.507	1082
5°	5 min:	1.022	230	21.458	-343299	19.65	29076
	10 min:	1.022	943	4.320	10599	7.835	16121
	15 min:	1.008	1028	0.599	810	4.837	-492
10°	5 min:	1.021	260	0.620	9537	1.884	-13500
	10 min:	1.021	956	0.487	2668	0.842	697
	15 min:	1.010	979	0.669	1006	0.785	1024

TABLE 6. Comparisons for 1 km cases, $\rho_{cm} = 909$ m, MEDIUM noise

		Batch Filter [13]		Manually-tuned EKF [16]		Adaptively-tuned EKF with k -biasing	
α	Δt	RMS	ρ_{cm}^* (m)	RMS	ρ_{cm}^* (m)	RMS	ρ_{cm}^* (m)
0°	5 min:	1.020	-1318	6.831	693696	8.238	613209
	10 min:	1.021	1001	4.017	-39847	11.36	104116
	15 min:	1.008	1521	0.952	1423	3.638	566
5°	5 min:	1.020	-1364	13.007	910863	6.816	203867
	10 min:	1.021	950	3.101	58191	3.533	56500
	15 min:	1.008	1472	0.800	970	2.489	6855
10°	5 min:	1.021	3381	13.075	918297	6.842	204010
	10 min:	1.021	1236	3.115	58121	3.541	56510
	15 min:	1.010	1416	0.799	840	2.491	6734

TABLE 7. Comparisons for 1 km cases, $\rho_{cm} = 909$ m, HIGH noise

		Batch Filter [13]		Manually-tuned EKF [16]		Adaptively-tuned EKF with k -biasing	
α	Δt	RMS	ρ_{cm}^* (m)	RMS	ρ_{cm}^* (m)	RMS	ρ_{cm}^* (m)
0°	5 min:	1.015	-892	0.473	20009	2.342	-8226
	10 min:	1.023	840	0.677	7081	1.273	2355
	15 min:	1.006	1003	0.594	1502	0.9346	963
5°	5 min:	1.020	-1432	8.636	1743440	4.763	-157130
	10 min:	1.021	1096	2.381	90619	4.373	119816
	15 min:	1.009	1950	0.680	1533	3.238	930
10°	5 min:	1.021	-8401	8.756	1784948	4.787	-161501
	10 min:	1.022	1509	2.386	91278	4.380	119851
	15 min:	1.011	2196	0.679	1458	3.238	744

TABLE 8. Comparisons for 10 km cases, $\rho_{cm} = 9091$ m, LOW noise

		Batch Filter [13]		Manually-tuned EKF [16]		Adaptively-tuned EKF with k -biasing	
α	Δt	RMS	ρ_{cm}^* (m)	RMS	ρ_{cm}^* (m)	RMS	ρ_{cm}^* (m)
0°	5 min:	1.022	8423	17.910	-591062	6.060	-217109
	10 min:	1.025	9192	1.382	22633	0.4890	8391
	15 min:	1.010	9339	0.637	10154	0.6134	9632
5°	5 min:	1.021	7948	11.251	26732	11.77	53852
	10 min:	1.025	8714	5.229	14630	5.429	13736
	15 min:	1.065	8845	1.755	9770	2.720	12807
10°	5 min:	1.021	7444	35.889	-1443476	12.54	551718
	10 min:	1.195	8406	0.370	27736	1.721	13200
	15 min:	1.028	8267	0.604	9959	1.747	8343

TABLE 9. Comparisons for 10 km cases, $\rho_{cm} = 9091$ m, MEDIUM noise

		Batch Filter [13]		Manually-tuned EKF [16]		Adaptively-tuned EKF with k -biasing	
α	Δt	RMS	ρ_{cm}^* (m)	RMS	ρ_{cm}^* (m)	RMS	ρ_{cm}^* (m)
0°	5 min:	1.020	6801	0.544	-2396	0.6496	9091
	10 min:	1.022	9179	0.472	19235	0.5880	15966
	15 min:	1.008	9787	0.657	12817	1.050	22614
5°	5 min:	1.020	6341	4.986	-360337	14.66	1506834
	10 min:	1.021	8708	2.010	21618	7.127	68631
	15 min:	1.010	9294	0.780	10351	2.398	6134
10°	5 min:	1.020	5842	4.986	-360842	14.24	1383031
	10 min:	1.022	8274	2.010	20967	9.143	115028
	15 min:	1.016	8855	0.779	9671	2.926	4684

TABLE 10. Comparisons for 10 km cases, $\rho_{cm} = 9091$ m, HIGH noise

		Batch Filter [13]		Manually-tuned EKF [16]		Adaptively-tuned EKF with k -biasing	
α	Δt	RMS	ρ_{cm}^* (m)	RMS	ρ_{cm}^* (m)	RMS	ρ_{cm}^* (m)
0°	5 min:	1.015	7211	0.380	25179	0.2834	10359
	10 min:	1.023	8992	0.478	14181	0.3606	10416
	15 min:	1.006	9225	0.529	10105	0.4563	9186
5°	5 min:	1.020	6301	18.581	1603925	6.635	-1426637
	10 min:	1.021	8888	0.997	148312	0.8132	71679
	15 min:	1.010	9791	0.758	10630	0.6790	10518
10°	5 min:	1.020	5811	18.580	1603099	6.634	-1427007
	10 min:	1.021	8450	0.996	147601	0.8133	71021
	15 min:	1.011	9355	0.758	10014	0.6795	9873

TABLE 11. Comparisons for 50 km cases, $\rho_{cm} = 45455$ m, LOW noise

		Batch Filter [13]		Manually-tuned EKF [16]		Adaptively-tuned EKF with k -biasing	
α	Δt	RMS	ρ_{cm}^* (m)	RMS	ρ_{cm}^* (m)	RMS	ρ_{cm}^* (m)
0°	5 min:	1.022	44523	7.125	-255455	3.986	-64684
	10 min:	1.027	45385	1.066	51432	0.4422	45428
	15 min:	1.023	45659	0.890	46422	0.6646	44962
5°	5 min:	1.017	42148	76.441	1804829	2.504	59790
	10 min:	1.035	42994	12.660	-20485	1.207	43754
	15 min:	1.844	43146	4.399	42729	1.220	45149
10°	5 min:	1.016	39625	270.15	-5901658	3.873	46189
	10 min:	1.105	40795	14.464	33030	1.976	42401
	15 min:	3.202	40910	0.503	46430	1.725	40072

TABLE 12. Comparisons for 50 km cases, $\rho_{cm} = 45455$ m, MEDIUM noise

		Batch Filter [13]		Manually-tuned EKF [16]		Adaptively-tuned EKF with k -biasing	
α	Δt	RMS	ρ_{cm}^* (m)	RMS	ρ_{cm}^* (m)	RMS	ρ_{cm}^* (m)
0°	5 min:	1.021	42789	5.219	-302465	13.13	648210
	10 min:	1.022	45482	0.619	43857	9.663	194554
	15 min:	1.008	46154	0.653	49841	4.583	44944
5°	5 min:	1.019	40517	0.534	-138322	12.87	1202841
	10 min:	1.021	43138	0.696	62693	8.772	144106
	15 min:	1.054	43703	0.540	48204	3.384	43042
10°	5 min:	1.019	38056	0.345	-217184	1.432	-691193
	10 min:	1.022	40931	0.693	58296	0.5688	45995
	15 min:	1.178	41358	0.540	44817	0.7569	44486

TABLE 13. Comparisons for 50 km cases, $\rho_{cm} = 45455$ m, HIGH noise

		Batch Filter [13]		Manually-tuned EKF [16]		Adaptively-tuned EKF with k -biasing	
α	Δt	RMS	ρ_{cm}^* (m)	RMS	ρ_{cm}^* (m)	RMS	ρ_{cm}^* (m)
0°	5 min:	1.020	42834	2.775	1758469	6.549	-1435114
	10 min:	1.022	45584	0.732	142976	0.8103	107429
	15 min:	1.009	46644	0.518	50734	0.6709	48181
5°	5 min:	1.019	40629	3.369	2836331	19.21	3636757
	10 min:	1.021	43221	0.771	169977	0.9604	77643
	15 min:	1.022	44137	0.519	48170	0.8773	45485
10°	5 min:	1.019	38232	5.070	5227532	153.7	7650025
	10 min:	1.022	41013	0.938	203335	39.36	-1267781
	15 min:	1.058	41908	0.528	46766	31.57	30505

TABLE 14. Comparisons for 1 km UP cases, $\rho_{cm} = -909$ m, LOW noise

		Batch Filter [13]		Manually-tuned EKF [16]		Adaptively-tuned EKF with k -biasing	
α	Δt	RMS	ρ_{cm}^* (m)	RMS	ρ_{cm}^* (m)	RMS	ρ_{cm}^* (m)
0°	5 min:	1.022	-1532	65.567	1254150	15.31	18527
	10 min:	1.022	-833	5.161	-50243	7.075	26939
	15 min:	1.006	-761	0.903	-1122	4.110	118
5°	5 min:	1.022	-1484	21.456	-344736	19.65	27320
	10 min:	1.022	-785	4.320	8959	7.835	14476
	15 min:	1.006	-712	0.600	-804	4.835	-2144
10°	5 min:	1.022	-1532	21.456	-344685	19.65	27378
	10 min:	1.022	-740	4.320	9024	7.835	14542
	15 min:	1.007	-688	0.600	-736	4.836	-2069

TABLE 15. Comparisons for 1 km UP cases, $\rho_{cm} = -909$ m, MEDIUM noise

		Batch Filter [13]		Manually-tuned EKF [16]		Adaptively-tuned EKF with k -biasing	
α	Δt	RMS	ρ_{cm}^* (m)	RMS	ρ_{cm}^* (m)	RMS	ρ_{cm}^* (m)
0°	5 min:	1.020	-3121	3.225	654906	0.8382	108676
	10 min:	1.021	-809	4.278	-40633	8.219	138718
	15 min:	1.008	-318	0.943	-1744	8.659	-20563
5°	5 min:	1.020	-3074	8.911	638134	10.39	763366
	10 min:	1.021	-757	3.134	33660	9.381	94157
	15 min:	1.008	-269	0.833	-624	3.203	-606
10°	5 min:	1.020	-3025	8.911	638192	10.39	763419
	10 min:	1.021	-709	3.134	33726	9.381	94216
	15 min:	1.008	225	0.833	-624	3.203	-540

TABLE 16. Comparisons for 1 km UP cases, $\rho_{cm} = -909$ m, HIGH noise

		Batch Filter [13]		Manually-tuned EKF [16]		Adaptively-tuned EKF with k -biasing	
α	Δt	RMS	ρ_{cm}^* (m)	RMS	ρ_{cm}^* (m)	RMS	ρ_{cm}^* (m)
0°	5 min:	1.020	-3194	11.369	277325	2.556	-2158
	10 min:	1.021	-683	2.465	124955	2.705	204906
	15 min:	1.009	-155	0.764	-1779	3.004	112275
5°	5 min:	1.020	-3149	7.018	2823610	4.762	-158748
	10 min:	1.021	-637	0.728	67245	4.373	118088
	15 min:	1.009	203	0.612	-1209	3.237	-1239
10°	5 min:	1.020	-3100	7.073	1424384	5.194	198245
	10 min:	1.021	-593	2.486	71591	4.528	144550
	15 min:	1.008	246	0.679	-901	3.265	-836

6. CONCLUSIONS

In summary, this study generated interesting and unique results for the quick-look identification methodology presented for identifying a satellite as being a member of a TSS using an EKF. The 2nd Stage TSS identification method used for both the manually-tuned EKF [15] and the adaptive EKF provided correct and quick identification of the tracked satellite. Both EKFs were sufficient in producing accurate results within the 15 minute time span. Where at least 15 minutes of data is processed, identification of a tethered satellite as part of a TSS can almost certainly be made.

One major disadvantage to using either EKF is that the results are very sensitive to the filter tuning parameters. Specifically, the choice of the *a priori* covariance and process noise parameters greatly affect the accuracy of the outcome of the filter. For the manually-tuned EKF cases, both parameters were manually-tuned which contributed to the difficulty of achieving acceptable filter performance. The adaptive EKF's filter tuning was slightly more automated with the addition of the biasing function and took advantage of using the *a priori* covariance found in the best manually-tuned cases. This required that only the process noise matrix be determined for the adaptively-tuned cases.

Finding the appropriate biasing function to use for tuning adaptive EKF cases depends on the level of error expected during process noise; and in this study, how accurately tuned the *a priori* covariance was from the manually-tuned cases. Selecting the appropriate biasing function form and variation of the form can be tedious, but

through experience with filter tuning the appropriate function can more easily be determined. Once the proper biasing function is selected, it is more advantageous when compared to the manually-tuned EKF because the process noise is updated each time an observation is processed in the adaptive EKF, rather than remaining constant throughout the analysis when using a manually-tuned filter.

Comparing the results of both EKFs to those of the batch filter, shows that a batch filter can be used to identify a tethered satellite more quickly than the EKFs can. Although the EKFs provided more accurate results than those found in the batch filter, the EKFs required more observations to do so.

Several recommendations can be made for future use of EKFs in identifying a satellite as a member of a TSS. In addition to using the most accurate data available to achieve optimum results, it is highly advised that at least 15 minutes of observation data be used in the 2nd Stage identification process. This observation data should be recorded as often as possible, since observations are processed by the adaptive EKF at each time step.

With the application of the adaptive EKF in this study, satisfying results were achieved; however additional analysis can be performed to streamline the entire tuning process. An iterative tuning process can be established when an EKF is required or desired for use in any study. This can be achieved by establishing an iteration procedure for any parameters needing to be tuned, such as the *a priori* covariance, the biasing function form and variation or any other parameter requiring tuning. Critical output values can be monitored within defined tolerances so that the desired filter performance can be achieved.

An iterative tuning procedure would benefit in the use of EKFs since it would alleviate the need for a trial and error process, which has traditionally been the means for tuning an EKF. However, extensive analysis must be performed early in the study when defining the iteration details. More effort may be required in the setup of an iterative process of this nature, but the caliber of the results achieved along with the ease of the tuning process would produce a useful and effective software solution where the application of EKFs are needed.

REFERENCES

1. Asher, T. A., D. G. Boden, and R. J. Tegtmeier, "Tethered satellites: The orbit determination problem and Missile Early Warning Systems," AIAA Paper 88-4284, *AIAA/AAS Astrodynamics Conference*, Minneapolis, MN, August 15-17, 1988.
2. Hoots, F. R., Roehrich, R. L., and Szebehely, V. G., "Space Shuttle Tethered Satellite Analysis," Directorate of Astrodynamics, Peterson AFB, CO, August 1983.
3. Qualls, C., and Cicci, D. A., "Preliminary Orbit Determination of a Tethered Satellite," Paper AAS 00-191, presented at the AAS/AIAA Astrodynamics Specialist Conference, Clearwater, FL, January 23-26, 2000.
4. Qualls, C., "Preliminary Orbit Determination of a Tethered Satellite," AU MS Thesis, 2000.
5. Kessler, S. A., and Cicci, D. A., "Filtering Methods for the Orbit Determination of a Tethered Satellite," *The Journal of the Astronautical Sciences*, Vol. 45, No. 3, July-September 1997, pp. 263-278.
6. Cicci, D. A., Lovell, T. A., and Qualls, C., "A Filtering Method for the Identification of a Tethered Satellite," *The Journal of the Astronautical Sciences*, Vol. 49, No. 2., April-June 2001, pp. 309-326.
7. Cicci, D. A., Qualls, C., and Lovell, T. A., "A Look at Tethered Satellite Identification Using Ridge-Type Estimation Methods," Paper AAS 99-415, presented at the AAS/AIAA Astrodynamics Specialist Conference, Girdwood, AK, August 16-19, 1999.
8. Cochran, J. E., Jr., Cho, S., Cheng, Y-M, and Cicci, D. A., "Dynamics and Orbit Determination of Tethered Satellite Systems," *The Journal of the Astronautical Sciences*, Vol. 46, No. 2, April-June 1998, pp. 177-194.
9. Cho, S., Cochran, J. E., Jr., and Cicci, D. A., "Modeling Tethered Satellite Systems for Detection and Orbit Determination," *The Journal of the Astronautical Sciences*, Vol. 48, No. 1, January-March 2000, pp. 89-108

10. Cochran, J. E., Jr., Cho, S., Lovell, T. A., and Cicci, D. A., "Evaluation of the Information Contained in the Motion of One Satellite of a Two-Satellite Tethered System," *The Journal of the Astronautical Sciences*, Vol. 48, No.4, October-December 2000, pp. 477-493.
11. Cho, S., Cochran, J. E., Jr., and Cicci, D. A., "Approximation Solutions for Tethered Satellite Motion," *AIAA Journal of Guidance, Control, and Dynamics*, Vol. 24, No. 4, August 2001, pp. 746-754.
12. Cho, S., Cochran, J. E., Jr., and Cicci, D. A., "Identification and Orbit Determination of Tethered Satellite Systems," *Applied Mathematics and Computation*, Vol. 117, 2001, pp. 301-312.
13. Cicci, D. A., Cochran, J. E., Jr., Qualls, C., Lovell, T. A., "Quick-Look Identification and Orbit Determination of a Tethered Satellite," *The Journal of the Astronautical Sciences*, Vol. 50, No. 3, July-September 2002, pp. 339-353.
14. "TiPS: Tether Physics and Survivability Satellite Experiment" web pages, Naval Center for Space Technology, <http://hyperspace.nrl.navy.mil/TiPS/data.html>.
15. Cicci, D. A., Volovecky, E. J., Qualls, C., "Identification of a Tethered Satellite Using a Kalman Filter," AIAA Paper 04-165, *AIAA/AAS Astrodynamics Conference*, Maui, HI, March 2004.
16. Cicci, D. A., "An Adaptive Extended Kalman Filter for Angles-Only Tracking/Intercept Problems," *The Journal of the Astronautical Sciences*, Vol. 41, No. 3, July-September 1993, pp. 411-435.
17. Swerling, P. "First Order Propagation in a Stagewise Smoothing Procedure for Satellite Observations," *The Journal of the Astronautical Sciences*, Vol. 6, 1959, pp. 46-62.
18. Kalman, R. E., and Bucy, R. S., "New Results in Linear Filtering and Prediction Theory," *ASME Journal of Basic Engineering*, Vol. 83, 1961, pp.95-108.

APPENDIX A: TEST CASE DATA

TABLE 17. Test Case Data: No Tether ($\rho_{cm} = 0$)

Noise Level	f(k)	Δt	RMS	ρ_{cm}^* (m)	
LOW	$(k-1)^2$	5 min.	1.948E+7	-7408104	
		10 min.	26720	-1.358E+9	
		15 min.	15512	-1.227E+8	
	k	5 min.	9508	-4.909E+10	
		10 min.	536754	-3.489E+7	
		15 min.	776503	-1.381E+7	
	$1/(k+1)^{20}$	5 min.	0.2431	-2416	
		10 min.	0.4431	-39	
		15 min.	0.6860	93	
	$1/(k+1)^{21}$	5 min.	0.2431	-2416	
		10 min.	0.4433	-39	
		15 min.	0.6862	92	
	MEDIUM	(k-1)	5 min.	1.010E+8	-3.033E+9
			10 min.	304318	-4.504E+9
			15 min.	20177	-1.558E+9
k		5 min.	145829	-8.204E+8	
		10 min.	7.976E+7	-1.397E+9	
		15 min.	5595	-1.013E+9	
$1/(k+1)^{20}$		5 min.	0.2329	-6559	
		10 min.	0.3631	320	
		15 min.	0.7086	686	
$1/(k+1)^{21}$		5 min.	0.2329	-6559	
		10 min.	0.3631	320	
		15 min.	0.7086	685	
HIGH		(k-1)	5 min.	0.1572	258513
			10 min.	0.2502	556325
			15 min.	0.4262	613046
	k	5 min.	0.1531	31660	
		10 min.	0.2779	1264131	
		15 min.	0.8096	473790	
	$1/(k+1)^{19}$	5 min.	0.1879	-9622	
		10 min.	0.3622	551	
		15 min.	0.7058	1297	
	$1/(k+1)^{20}$	5 min.	0.1879	-9622	
		10 min.	0.3622	551	
		15 min.	0.7059	1297	

TABLE 18. Test Case Data: $\rho = 1$ km ($\rho_{cm} = 909$ m), LOW noise

α	f(k)	Δt	RMS	ρ_{cm}^* (m)	
0°	k ²	5 min.	79246	-2.629E+7	
		10 min.	54037	-6.210E+9	
		15 min.	15664	-1.004E+9	
	(k-1)	5 min.	9.770	185433	
		10 min.	18598	-8.038E+9	
		15 min.	90578	-8320845	
	1/(k+1) ⁸	5 min.	11.18	63636	
		10 min.	5.368	12295	
		15 min.	3.782	1397	
	1/k ⁸	5 min.	16.03	30885	
		10 min.	7.760	30051	
		15 min.	4.507	1082	
	5°	k	5 min.	1.582E+7	-3.289E+10
			10 min.	844865	-4796600
			15 min.	34161	-4.853E+8
k ²		5 min.	208974	-1.162E+8	
		10 min.	1.429E+7	-4.033E+8	
		15 min.	5381568	-2.482E+7	
1/(k+1) ⁶		5 min.	16.25	31850	
		10 min.	6.801	24515	
		15 min.	4.047	-766	
1/(k+1) ⁸		5 min.	19.65	29076	
		10 min.	7.835	16121	
		15 min.	4.837	-492	
10°		(k-1)	5 min.	41970	-1.039E+10
			10 min.	3316391	-8.432E+9
			15 min.	1190777	-1.641E+8
	k	5 min.	0.9509	-3578792	
		10 min.	9710738	-1.894E+8	
		15 min.	860739	-3.679E+7	
	1/(k+1) ¹⁹	5 min.	2.055	-14873	
		10 min.	2.096	-662	
		15 min.	0.697	1027	
	1/(k+1) ¹⁸	5 min.	1.884	-13500	
		10 min.	0.842	697	
		15 min.	0.785	1024	

TABLE 19. Test Case Data: $\rho = 1$ km ($\rho_{cm} = 909$ m), MEDIUM noise

α	f(k)	Δt	RMS	ρ_{cm}^* (m)	
0°	k	5 min.	103.1	1818062	
		10 min.	0.4188	46684	
		15 min.	105657	-4.427E+8	
	(k-1)	5 min.	22.26	-2.336E+7	
		10 min.	2.181	-84327	
		15 min.	5230	-2.208E+8	
	1/k ⁶	5 min.	4.723	161874	
		10 min.	4.876	74596	
		15 min.	3.059	506	
	1/(k+1) ¹³	5 min.	8.238	613209	
		10 min.	11.36	104116	
		15 min.	3.638	566	
	5°	k	5 min.	5.621	250947
			10 min.	3.045	325449
			15 min.	28066	-6080792
(k-1)		5 min.	5.628	358120	
		10 min.	2.998	449543	
		15 min.	1.092	486845	
1/(k+1) ⁵		5 min.	7.538	-225738	
		10 min.	3.755	44240	
		15 min.	2.625	7176	
1/(k+1) ⁴		5 min.	6.816	203867	
		10 min.	3.533	56500	
		15 min.	2.489	6855	
10°		(k-1)	5 min.	5.629	250800
			10 min.	3.046	324929
			15 min.	6938	-7375386
	k	5 min.	5.638	358068	
		10 min.	3.001	448444	
		15 min.	1.139	486206	
	1/k ⁷	5 min.	6.662	121095	
		10 min.	3.468	44970	
		15 min.	2.491	7993	
	1/(k+1) ⁴	5 min.	6.842	204010	
		10 min.	3.541	56510	
		15 min.	2.491	6734	

TABLE 20. Test Case Data: $\rho = 1$ km ($\rho_{cm} = 909$ m), HIGH noise

α	f(k)	Δt	RMS	ρ_{cm}^* (m)	
0°	k ²	5 min.	215727	-1.252E+8	
		10 min.	60705	-3.087E+8	
		15 min.	47348	-1.666E+8	
	(k-1)	5 min.	2.286E+7	-3.890E+8	
		10 min.	40120	-4.000E+8	
		15 min.	17875	-1.082E+8	
	1/k ¹⁶	5 min.	1.789	-3662	
		10 min.	1.131	2921	
		15 min.	0.7322	891	
	1/k ²⁰	5 min.	2.342	-8226	
		10 min.	1.273	2355	
		15 min.	0.9346	963	
	5°	k	5 min.	4.319	418352
			10 min.	4.249	196265
			15 min.	78.05	-6102592
(k-1)		5 min.	4.358	384777	
		10 min.	4.206	202737	
		15 min.	30.01	-724931	
1/k ⁵		5 min.	4.748	-259218	
		10 min.	4.354	113148	
		15 min.	3.245	3201	
1/(k+1) ³		5 min.	4.763	-157130	
		10 min.	4.373	119816	
		15 min.	3.238	930	
10°		k	5 min.	4.331	417880
			10 min.	4.253	196247
			15 min.	71.67	-6049962
	(k-1)	5 min.	4.370	376580	
		10 min.	4.213	202907	
		15 min.	29.36	-654351	
	1/k ⁵	5 min.	4.772	-263485	
		10 min.	4.362	113210	
		15 min.	3.245	3014	
	1/(k+1) ³	5 min.	4.787	-161501	
		10 min.	4.380	119851	
		15 min.	3.238	744	

TABLE 21. Test Case Data: $\rho = 10$ km ($\rho_{cm} = 9091$ m), LOW noise

α	f(k)	Δt	RMS	ρ_{cm}^* (m)	
0°	k ²	5 min.	9333	-1.945E+9	
		10 min.	16554	-4.025E+7	
		15 min.	16904	-5.611E+9	
	(k-1) ²	5 min.	10.79	187180	
		10 min.	4.014E+7	-6.773E+7	
		15 min.	9369	-3.998E+8	
	1/k ¹⁴	5 min.	34.75	-393739	
		10 min.	5.419	17539	
		15 min.	4.153	9784	
	1/k ⁹	5 min.	6.060	-217109	
		10 min.	0.4890	8391	
		15 min.	0.6134	9632	
	5°	k ²	5 min.	1384498	-1.951E+7
			10 min.	205806	-7.384E+8
			15 min.	29305	-4.252E+9
(k-1) ²		5 min.	9.251	174365	
		10 min.	27515	-7.132E+7	
		15 min.	38093	-2.057E+9	
1/k ⁶		5 min.	13.29	42465	
		10 min.	6.268	15103	
		15 min.	3.298	4459	
1/k ⁵		5 min.	11.77	53852	
		10 min.	5.429	13736	
		15 min.	2.720	12807	
10°		k	5 min.	17918	-7.760E+8
			10 min.	25090	-1.508E+7
			15 min.	211137	-2.656E+9
	(k-1)	5 min.	46356	-1.644E+8	
		10 min.	556165	-3.057E+8	
		15 min.	24391	-1.139E+7	
	1/(k+1) ⁹	5 min.	45.71	-1787109	
		10 min.	1.496	15401	
		15 min.	1.254	10057	
	1/(k+1) ⁸	5 min.	12.54	551718	
		10 min.	1.721	13200	
		15 min.	1.747	8343	

TABLE 22. Test Case Data: $\rho = 10$ km ($\rho_{cm} = 9091$ m), MEDIUM noise

α	f(k)	Δt	RMS	ρ_{cm}^* (m)	
0°	k	5 min.	17853	-2.590E+11	
		10 min.	184594	-1.598E+8	
		15 min.	10008	-4.272E+8	
	k ²	5 min.	1.557E+7	-3.012E+9	
		10 min.	157668	-1.627E+8	
		15 min.	107549	-4732578	
	1/(k+1) ¹²	5 min.	1.006	65842	
		10 min.	0.6383	15992	
		15 min.	0.8980	10545	
	1/(k+1) ⁶	5 min.	0.6496	9091	
		10 min.	0.5880	15966	
		15 min.	1.050	22614	
	5°	(k-1) ²	5 min.	3.197	256493
			10 min.	17718	-8.348E+8
			15 min.	5936	-3.960E+9
(k-1)		5 min.	3.191	254015	
		10 min.	1.979	802715	
		15 min.	44311	-3.185E+8	
1/(k+1) ¹³		5 min.	14.24	1383702	
		10 min.	9.139	115611	
		15 min.	2.928	5340	
1/k ²¹		5 min.	14.66	1506834	
		10 min.	7.127	68631	
		15 min.	2.398	6134	
10°		k	5 min.	3.158	362342
			10 min.	2.540	836567
			15 min.	449341	-2.630E+9
	(k-1)	5 min.	3.191	253351	
		10 min.	2.109	1030993	
		15 min.	9.151	-1709413	
	1/k ²⁰	5 min.	15.07	1567105	
		10 min.	4.800	6979	
		15 min.	2.038	14877	
	1/(k+1) ¹³	5 min.	14.24	1383031	
		10 min.	9.143	115028	
		15 min.	2.926	4684	

TABLE 23. Test Case Data: $\rho = 10$ km ($\rho_{cm} = 9091$ m), HIGH noise

α	f(k)	Δt	RMS	ρ_{cm}^* (m)	
0°	(k-1) ²	5 min.	86174	-2.786E+11	
		10 min.	222068	-3.655E+8	
		15 min.	520551	-1.107E+9	
	k ²	5 min.	74891	-2.003E+8	
		10 min.	46188	-7.888E+7	
		15 min.	21370	-1.053E+8	
	1/(k+1) ²¹	5 min.	0.2406	11202	
		10 min.	0.4266	9307	
		15 min.	0.7085	8814	
	1/k ¹⁵	5 min.	0.2834	10359	
		10 min.	0.3606	10416	
		15 min.	0.4563	9186	
	5°	k	5 min.	4.735	513295
			10 min.	2.552	250591
			15 min.	3.387	545368
(k-1)		5 min.	4.336	79536	
		10 min.	2.047	375226	
		15 min.	1.050	343727	
1/(k+1) ⁶		5 min.	9.441	-800925	
		10 min.	0.8150	54226	
		15 min.	0.7375	11919	
1/k ¹⁰		5 min.	6.635	-1426637	
		10 min.	0.8132	71679	
		15 min.	0.6790	10518	
10°		k	5 min.	4.735	512591
			10 min.	2.553	249809
			15 min.	3.558	564122
	(k-1)	5 min.	4.336	78918	
		10 min.	2.048	374348	
		15 min.	1.074	340145	
	1/(k+1) ⁶	5 min.	9.441	-801358	
		10 min.	0.8149	53564	
		15 min.	0.7352	11274	
	1/k ¹⁰	5 min.	6.634	-1427007	
		10 min.	0.8133	71021	
		15 min.	0.6795	9873	

TABLE 24. Test Case Data: $\rho = 50$ km ($\rho_{cm} = 45455$ m), LOW noise

α	f(k)	Δt	RMS	ρ_{cm}^* (m)	
0°	(k-1) ²	5 min.	5.395	231609	
		10 min.	801420	-4.4474E+11	
		15 min.	1.693E+7	-2.602E+8	
	k ²	5 min.	10994	-5502491	
		10 min.	16017	-1.009E+9	
		15 min.	264641	-3.167E+7	
	1/k ¹⁵	5 min.	2.604	57065	
		10 min.	0.4719	44662	
		15 min.	0.8280	45715	
	1/k ¹⁶	5 min.	3.986	-64684	
		10 min.	0.4422	45428	
		15 min.	0.6646	44962	
	5°	k ²	5 min.	1.446E+8	-2.454E+11
			10 min.	193956	-3.943E+9
			15 min.	2604	-7301015
(k-1) ²		5 min.	5.396	228756	
		10 min.	42646	-3.877E+8	
		15 min.	51900	-5525326	
1/k ⁷		5 min.	2.438	64344	
		10 min.	1.186	45427	
		15 min.	1.186	49021	
1/k ⁸		5 min.	2.504	59790	
		10 min.	1.207	43754	
		15 min.	1.220	45149	
10°		k ²	5 min.	3.548	447265
			10 min.	8726927	-2.807E+8
			15 min.	3381018	-2.204E+8
	(k-1) ²	5 min.	864520	-1.155E+7	
		10 min.	4.396E+7	-3.929E+8	
		15 min.	76714	-4.701E+7	
	1/k ⁶	5 min.	0.8651	50501	
		10 min.	0.7711	47243	
		15 min.	0.5045	47104	
	1/k ¹⁰	5 min.	3.873	46189	
		10 min.	1.976	42401	
		15 min.	1.725	40072	

TABLE 25. Test Case Data: $\rho = 50$ km ($\rho_{cm} = 45455$ m), MEDIUM noise

α	f(k)	Δt	RMS	ρ_{cm}^* (m)
0°	k	5 min.	3.175	404529
		10 min.	1.878	225780
		15 min.	22242	-1.102E+7
	k ²	5 min.	2.675	675655
		10 min.	1315	-7.271E+7
		15 min.	2152	-9912064
	1/(k+1) ¹³	5 min.	10.448	753723
		10 min.	8.351	147276
		15 min.	3.649	49440
	1/(k+1) ¹⁴	5 min.	13.13	648210
		10 min.	9.663	194554
		15 min.	4.583	44944
5°	(k-1)	5 min.	3.192	291176
		10 min.	1.655	798882
		15 min.	2.886	892367
	k	5 min.	3.175	401593
		10 min.	1.569	690194
		15 min.	6.579	469003
	1/k ²⁰	5 min.	12.86	1324856
		10 min.	5.037	49065
		15 min.	2.499	52389
	1/(k+1) ¹³	5 min.	12.87	1202841
		10 min.	8.772	144106
		15 min.	3.384	43042
10°	(k-1) ²	5 min.	3.184	284810
		10 min.	1.354E+7	-1.763E+9
		15 min.	10182	-7.710E+7
	k ²	5 min.	2.455	726058
		10 min.	515473	-7.197E+7
		15 min.	6302	-1.803E+7
	1/(k+1) ¹¹	5 min.	44.32	3140658
		10 min.	2.368	-77223
		15 min.	1.104	46131
	1/(k+1) ⁷	5 min.	1.432	-691193
		10 min.	0.5688	45995
		15 min.	0.7569	44486

TABLE 26. Test Case Data: $\rho = 50$ km ($\rho_{cm} = 45455$ m), HIGH noise

α	f(k)	Δt	RMS	ρ_{cm}^* (m)	
0°	(k-1)	5 min.	4.350	117136	
		10 min.	2.048	439609	
		15 min.	51874	-3881839	
	k	5 min.	4.750	556965	
		10 min.	2.553	300542	
		15 min.	2.055	665919	
	1/k ¹⁴	5 min.	41.33	3.437E+7	
		10 min.	4.218	-115323	
		15 min.	1.140	48648	
	1/k ¹⁰	5 min.	6.549	-1435114	
		10 min.	0.8103	107429	
		15 min.	0.6709	48181	
	5°	k	5 min.	3.583	400650
			10 min.	665978	-2.094E+8
			15 min.	3679	-9128196
(k-1)		5 min.	4.119	291700	
		10 min.	1.945	529531	
		15 min.	1.295	356237	
1/k ¹³		5 min.	15.90	2601556	
		10 min.	0.7851	95354	
		15 min.	0.9108	46854	
1/(k+1) ⁸		5 min.	19.21	3636757	
		10 min.	0.9604	77643	
		15 min.	0.8773	45485	
10°		(k-1) ²	5 min.	19.54	-2344955
			10 min.	3.616	231902
			15 min.	26125	-4.056E+8
	(k-1)	5 min.	8.483	-1325513	
		10 min.	34868	-1.097E+9	
		15 min.	2647	-8848180	
	1/k ²⁰	5 min.	152.9	1.221E+7	
		10 min.	40.52	-1325599	
		15 min.	33.98	20924	
	1/(k+1) ¹²	5 min.	153.7	7650025	
		10 min.	39.36	-1267781	
		15 min.	31.57	30505	

TABLE 27. Test Case Data: $\rho = 1$ km up ($\rho_{cm} = -909$ m), LOW noise

α	f(k)	Δt	RMS	ρ_{cm}^* (m)	
0°	k	5 min.	19052	-2.120E+8	
		10 min.	34387	-3.174E+8	
		15 min.	21728	-9.479E+8	
	(k-1)	5 min.	12.19	186597	
		10 min.	1.384E+7	-2.584E+8	
		15 min.	50100	-5.576E+8	
	1/k ¹⁵	5 min.	61.00	-255588	
		10 min.	24.29	33578	
		15 min.	14.07	-2049	
	1/(k+1) ⁵	5 min.	15.31	18527	
		10 min.	7.075	26939	
		15 min.	4.110	118	
	5°	(k-1)	5 min.	12.74	187621
			10 min.	8.131E+7	-1.886E+9
			15 min.	38714	-2.556E+8
(k-1) ²		5 min.	11.79	177763	
		10 min.	36909	-4.148E+7	
		15 min.	1849706	-5546073	
1/(k+1) ⁶		5 min.	16.25	30146	
		10 min.	6.801	22862	
		15 min.	4.044	-2528	
1/(k+1) ⁸		5 min.	19.65	27320	
		10 min.	7.835	14476	
		15 min.	4.835	-2144	
10°		k ²	5 min.	174303	-5196165
			10 min.	10543	-3.563E+11
			15 min.	43525	-1.850E+9
	(k-1) ²	5 min.	11.79	177828	
		10 min.	82339	-7.497E+8	
		15 min.	407830	-2.402E+8	
	1/(k+1) ⁶	5 min.	16.25	30206	
		10 min.	6.801	22928	
		15 min.	4.044	-2450	
	1/(k+1) ⁸	5 min.	19.65	27378	
		10 min.	7.835	14542	
		15 min.	4.836	-2069	

TABLE 28. Test Case Data: $\rho = 1$ km up ($\rho_{cm} = -909$ m), MEDIUM noise

α	f(k)	Δt	RMS	ρ_{cm}^* (m)	
0°	k	5 min.	4.040	1711062	
		10 min.	332479	-5.537E+8	
		15 min.	9223	-2.146E+8	
	(k-1) ²	5 min.	9463021	-3.204E+10	
		10 min.	4138	-1.782E+9	
		15 min.	762	-5482947	
	1/k ¹²	5 min.	4.414	426439	
		10 min.	15.24	106843	
		15 min.	53.03	-54076	
	1/(k-1) ³	5 min.	0.8382	108676	
		10 min.	8.219	138718	
		15 min.	8.659	-20563	
	5°	(k-1)	5 min.	6.645	252247
			10 min.	3.381	232577
			15 min.	59352	-1.100E+7
k		5 min.	6.614	358337	
		10 min.	3.326	337699	
		15 min.	1.071	492506	
1/(k+1) ¹⁴		5 min.	14.62	699033	
		10 min.	12.01	164880	
		15 min.	4.301	-9869	
1/(k+1) ¹³		5 min.	10.39	763366	
		10 min.	9.381	94157	
		15 min.	3.203	-606	
10°		k ²	5 min.	6.614	493022
			10 min.	766.6	-1.042E+8
			15 min.	153437	-6506473
	k	5 min.	6.614	358405	
		10 min.	3.326	337777	
		15 min.	1.065	492748	
	1/(k+1) ⁴	5 min.	6.934	119266	
		10 min.	3.643	56365	
		15 min.	2.568	4557	
	1/(k+1) ¹³	5 min.	10.39	763419	
		10 min.	9.381	94216	
		15 min.	3.203	-540	

TABLE 29. Test Case Data: $\rho = 1$ km up ($\rho_{cm} = -909$ m), HIGH noise

α	f(k)	Δt	RMS	ρ_{cm}^* (m)	
0°	(k-1)	5 min.	3.266	1274895	
		10 min.	2.674	1734528	
		15 min.	3874	-9.433E+7	
	k	5 min.	2.351	633480	
		10 min.	5228083	-2.215E+9	
		15 min.	6232	-5.042E+7	
	1/(k-1) ⁴	5 min.	2.042	-8681	
		10 min.	2.923	191447	
		15 min.	3.063	101456	
	1/(k-1) ²	5 min.	2.556	-2158	
		10 min.	2.705	204906	
		15 min.	3.004	112275	
	5°	k	5 min.	4.319	416463
			10 min.	4.250	194422
			15 min.	208.4	-6786659
(k-1)		5 min.	4.358	382826	
		10 min.	4.207	200965	
		15 min.	31.04	-846237	
1/k ⁴		5 min.	4.599	342338	
		10 min.	4.329	140397	
		15 min.	3.207	991	
1/(k+1) ³		5 min.	4.762	-158748	
		10 min.	4.373	118088	
		15 min.	3.237	-1239	
10°		k	5 min.	4.501	445663
			10 min.	4.313	195575
			15 min.	44.87	-5428452
	(k-1)	5 min.	4.601	386415	
		10 min.	4.246	202680	
		15 min.	29.96	-702344	
	1/k ⁵	5 min.	5.374	-307660	
		10 min.	4.571	115868	
		15 min.	3.322	-796	
	1/k ⁴	5 min.	5.194	198245	
		10 min.	4.528	144550	
		15 min.	3.265	-836	